ChemPubSoc Europe

DOI: 10.1002/cphc.201501089

CHEMPHYSCHEM Articles

Special Issue

Site-Specific Dynamics of β-Sheet Peptides with ^{D}Pro–Gly Turns Probed by Laser-Excited Temperature-Jump Infrared Spectroscopy

Alexander Popp,[a] David Scheerer,[a] Heng Chi,[b] Timothy A. Keiderling,[c] and Karin Hauser*[a]

Dedicated to Professor Wolfgang Zinth on the occasion of his 65th birthday

Turn residues and side-chain interactions play an important role for the folding of β-sheets. We investigated the conformational dynamics of a three-stranded β-sheet peptide (^{D}P^{D}P) and a two-stranded β-hairpin (WVYY–^{D}P) by time-resolved temperature-jump (*T*-jump) infrared spectroscopy. Both peptide sequences contain ^{D}Pro–Gly residues that favor a tight β-turn. The three-stranded β-sheet (Ac-VFITS^{D}*PG*KTYTEV^{D}*PG*OKILQ–NH_2) is stabilized by the turn sequences, whereas the β-hairpin (SWTVE^{D}*PG*KYTYK–NH_2) folding is assisted by both the turn sequence and hydrophobic cross-strand interactions. Relaxation times after the *T*-jump were monitored as a function of temperature and occur on a sub-microsecond time scale, ^{D}P^{D}P being faster than WVYY–^{D}P. The Xxx–^{D}Pro tertiary amide provides a detectable IR band, allowing us to probe the dynamics site-specifically. The relative importance of the turn versus the intrastrand stability in β-sheet formation is discussed.

1. Introduction

The early kinetic steps in protein folding provide insights into the molecular driving forces of protein structure formation. Particular interest in understanding the factors affecting β-sheet formation is prompted by the fact that β-sheet structures are often involved or even initiate protein aggregation. Peptides are ideal model systems to assess the relative importance of individual residues in forming a stable β-sheet. A complex balance of factors is involved in structural stabilization, that is, hydrogen bonding, side chain–side chain interactions, and turn geometry, and varying the sequence can systematically test the impact of specific interactions on the structure. However, the generation of nonaggregating, water-soluble β-sheet models is not trivial. Isolated sequences that form sheet segments in folded proteins do not often result in independent, soluble β-sheet structures, as tertiary contacts and, in particular, hydrophobic interactions in the protein fold are missing and these are important for stability.

Model sequences of β-hairpins and three-stranded β-sheets that are stable in aqueous solutions have been designed by utilizing residues that favor a turn, cross-strand hydrophobic interactions, or both.[1] One example of a turn-initiated folding of a three-stranded β-sheet model is the sequence Ac-VFITS^{D}*PG*KTYTEV^{D}*PG*OKILQ-NH_2 (abbreviated to ^{D}P^{D}P), which was originally designed by Gellman and Schenck.[2] The two ^{D}Pro–Gly segments promote the formation of tight β-turns, resulting in a structure having two β-hairpins with one strand in common (Scheme 1). The sequence was designed to have a net charge of $\geq +2$ at acidic pH to discourage aggregation and to form a monomeric triple-stranded antiparallel β-sheet in aqueous solutions. Its β-sheet structure was confirmed by

[a] Dr. A. Popp, D. Scheerer, Prof. K. Hauser
Department of Chemistry
University of Konstanz
78457 Konstanz (Germany)
Fax: (+49) 7531-88-3139
E-mail: Karin.Hauser@uni-konstanz.de

[b] Dr. H. Chi
Department of Pharmacy and Health Management
Jiangsu Food and Pharmaceutical Science College
4 E. Meicheng Rd. Huai'an, Jiangsu Province, 223003 (P. R. China)

[c] Prof. T. A. Keiderling
Department of Chemistry
University of Illinois at Chicago
845 W. Taylor St., Chicago, Illinois 60607-7061 (USA)

Supporting Information for this article can be found under http://dx.doi.org/10.1002/cphc.201501089.

An invited contribution to a Special Issue on Fast Spectroscopy: Biosystems.

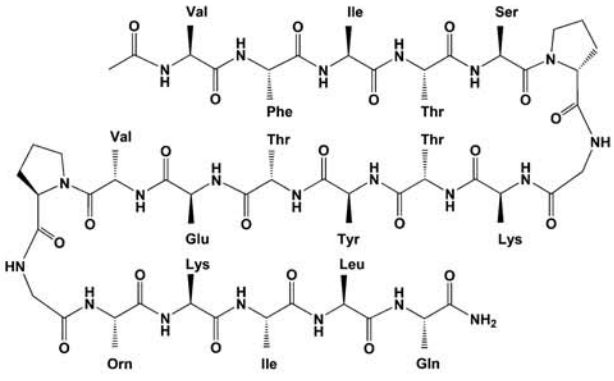

Scheme 1. The sequence of ^{D}P^{D}P. The peptide consists of 20 amino acids with three antiparallel strands that are connected by two highly constrained ^{D}Pro–Gly turns.

NMR spectroscopy,[2] and subsequently, by equilibrium infrared (IR), vibrational circular dichroism (VCD), and fluorescence resonance energy transfer (FRET) studies.[3]

Kinetic studies of β-sheet model peptides with ^{D}Pro–Gly turns have shown folding and refolding dynamics on a sub-microsecond time scale by using various methodological approaches.[4] Besides the turns, cross-strand interactions between nonsequential residue side chains can assist β-sheet folding. For example, Trp residues have been utilized to stabilize small β-hairpin peptides through cross-strand hydrophobic interactions.[1a,5] Side-chain interactions have significant impact on conformational stability and dynamics, as we have shown for variants based on Cochran's Trpzip2 sequence (SWTWE*NG*KWTWK–NH_2), which has an Asn–Gly turn and four Trp (W) residues that form cross-strand pairs, due to strong edge-on-face hydrophobic interactions. Substitutions of the Trp–Trp pairs by either Tyr or Val destabilize the structure and have an influence on the folding pathway.[5c,6] Furthermore, we studied different turn residues with respect to their role in β-hairpin conformation and stability. Substitution of Asn–Gly with a ^{D}Pro–Gly sequence stabilizes the turn, but at the same time, the β-structure (cross-strand H bonds) becomes less stable, owing to the constraints of the ^{D}Pro–Gly turn.[7] This demonstrates that turn and sheet residues can have a significant impact on β-sheet folding. Here, we designed a β-hairpin with the sequence SWTVE^{D}*PG*KYTYK–NH_2 (abbreviated to WVYY-^{D}P), which combines turn-enhanced folding by the use of a ^{D}Pro-Gly turn as well as strand-assisted folding by cross-strand interactions of pairs of hydrophobic residues, Trp–Tyr and Val–Tyr.

Time-resolved infrared spectroscopy (TRIR) is a versatile technique for the analysis of peptide and protein folding dynamics, as it is structure sensitive and offers high temporal resolution. Whereas stopped-flow methods are restricted to folding events on the millisecond or slower time scale, due to limitations of rapid mixing, laser-initiated relaxation measurements can access faster kinetics. The dead time of such experiments is effectively limited only by the length of the excitation pulses and the response function of the detection electronics and is short enough to access the fast processes in peptide and protein folding.[8] We utilize a laser-excited temperature-jump (*T*-jump) technique that shifts the thermal equilibrium and monitors the relaxation of the excited system to a new equilibrium at the higher temperature. An appropriate infrared laser pulse excites solvent vibrational modes, the fast nonradiative relaxation of which thereby generates a rapid *T*-jump. Thermalization of the solvent occurs on a picosecond timescale[9] and is completed within the width of the nanosecond excitation pulse used in our spectrometer setup. By following the time course of the spectral changes in the amide I′ region (mainly the C=O stretching vibrations of the polypeptide backbone), the relaxation dynamics of the backbone structural rearrangement can be monitored.

In this study, we analyze a three-stranded β-sheet and β-hairpin with ^{D}Pro–Gly turns. The Xxx–^{D}Pro amide yields a distinct amide I′ component and was used to probe the dynamics site-specifically for the turn-to-strand link, as well as monitoring the overall β-hairpin decay and the rise of disordered structure. Relaxation times were determined as a function of temperature to provide insights into the interplay between turn- and sheet-stabilizing residues and their contribution to folding dynamics. Modifications and improvements of our current *T*-jump laser IR setup are described in detail in the Experimental Section.

2. Results

2.1. Three-Stranded β-Sheet ^{D}P^{D}P

FTIR spectra were used to monitor the thermal unfolding of ^{D}P^{D}P under equilibrium conditions. Figure 1 shows a set of temperature-dependent and solvent-corrected FTIR spectra. At low temperatures, ^{D}P^{D}P has an antiparallel β-sheet structure, as seen by the characteristic amide I′ absorbance, having a strong component with a maximum at 1636 cm^{-1} and a weak component, which is observed as a shoulder at 1675 cm^{-1} (Figure 1a). In addition, a shoulder is observed at 1610 cm^{-1}, which can be attributed to the Xxx–^{D}Pro tertiary amides that sequentially precede the two β-turns.[3,10] This band component can be used as a site-specific probe that, for ^{D}P^{D}P, represents the links of strand 1 with the first turn (Ser–^{D}Pro) and strand 2 with the second turn (Val–^{D}Pro; Scheme 1).

The amide I′ maximum at 1636 cm^{-1} shifts to 1643 cm^{-1} upon heating, thus indicating unfolding to a disordered structure. The thermal transition, which was monitored by the amide I′ frequency shift, lacks a sigmoidal shape; consequently

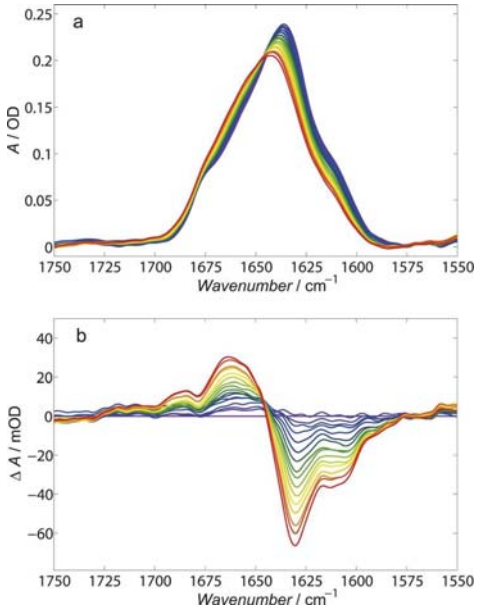

Figure 1. Equilibrium FTIR absorbance (a) and difference (b) spectra of ^{D}P^{D}P at acidic pD as a function of temperature. The temperature variation between 7 (blue spectrum) and 85 °C (red spectrum) in steps of $\Delta T \approx 5$ °C reveals the increase in the disordered structure at 1663 cm^{-1}, the loss of β-sheet at 1630 cm^{-1}, and additionally a decrease of the Xxx-.^{D}Pro amide I′ component corresponding to the turn region at 1612 cm^{-1}.

the fitted transition temperature, $T_m = 55\,^{\circ}C$, is subject to larger errors. We performed the measurements at acidic pD, where thermal unfolding and refolding is completely reversible, which is not the case at neutral pD (data not shown). Reversibility is a prerequisite for the *T*-jump measurements, as several thousands of transients are averaged. Difference spectra (Figure 1 b) are a useful means to better identify the major absorbance changes upon thermal unfolding and were used to select the probe wavenumbers for the *T*-jump experiments, that is, 1630 cm^{-1} to monitor the decay of the β-hairpin structure, 1612 cm^{-1} for the dynamics of the turn-to-strand link, and 1663 cm^{-1} for the increase in the disordered structure.

T-jump studies were performed with our home-built quantum cascade laser (QCL)-based *T*-jump spectrometer. The current design, improvements, measurement procedure, and the data analysis approach used are described in detail in the Experimental Section. Transients were measured at three different probe wavenumbers described above as a function of temperature between 6 and 50 °C. Figure 2 shows the relaxation

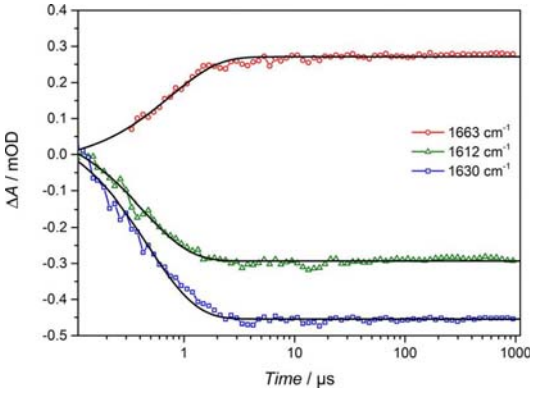

Figure 2. Relaxation of $^{D}P^{D}P$ after the laser-excited temperature-jump, shown as an example for one temperature (18 °C) at each wavenumber probed. The transient signal reflects the decay of the β-sheet and Xxx–^{D}Pro turn region (1630 and 1612 cm^{-1}, blue and green, respectively) and the increase in the disordered structure (1663 cm^{-1}, red). Shorter time kinetics for the latter were distorted by cavitation interference.

kinetics for $^{D}P^{D}P$ at $T \approx 8\,^{\circ}C$ (the final temperature after the *T*-jump). The signal amplitudes when the probe was tuned to the turn (1612 cm^{-1}) and β-sheet (1630 cm^{-1}) amide I′ components both have negative amplitudes, but different magnitudes, as expected. Relaxation time constants, which were determined for different final temperatures, are shown in Figure 3 in the form of an Arrhenius plot. All values are given in Table S2 in the Supporting Information. The relaxation time constants probed for the β-sheet (Figure 3, blue data points) and the turn region (Figure 3, green data points) are similar and reveal similar temperature dependencies. It becomes obvious that the time constants for the increase of the disordered structure are slower overall than those for the loss of sheets or change in the turn, and thus, correspond to lower rates in the Arrhenius plot (Figure 3, red data points). The apparent activation energies derived from fits of the rate constants to the

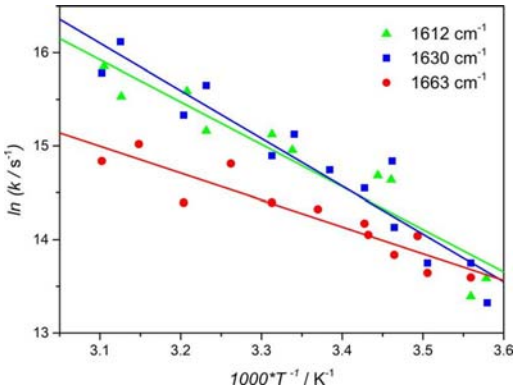

Figure 3. Arrhenius plot for the relaxation kinetics of $^{D}P^{D}P$ shows the temperature dependencies of the rate constants measured at selected wavenumbers (1630 cm^{-1}, blue squares: β-sheet; 1612 cm^{-1}, green triangles: Xxx-^{D}Pro turn region; 1663 cm^{-1}, red dots: disordered structure). The temperature refers to the final peptide temperature after the *T*-jump. Apparent activation energies were obtained by fitting each data set to the Arrhenius equation: $\ln(k) = \frac{-E_a}{RT} + \ln(A)$.

Table 1. Relaxation times τ (μs) at ~25 °C (final peptide temperature) and apparent activation energies E_a (kJ mol^{-1}) for $^{D}P^{D}P$, WVYY-^{D}P.

		$^{D}P^{D}P$[b]	WVYY-^{D}P[b]
τ [μs][a]			
	^{D}P-band	0.32	0.53
	β-band	0.27	0.41
	disordered	0.60	0.81
E_a [kJ mol^{-1}]			
	^{D}P-band	37.8 ± 4.5	49.8 ± 3.3
	β-band	42.5 ± 4.3	48.3 ± 3.7
	disordered	23.8 ± 3.0	36.8 ± 3.1

[a] Relaxation times for all studied temperatures can be found in Tables S1 and S2 in the Supporting Information, for $^{D}P^{D}P$ and WYYY–^{D}P, respectively. [b] The error of repeated measurements is in the range of 150 ns.

Arrhenius relationship are summarized in Table 1. The disorder rate constants also show less temperature dependence, and thus, a smaller apparent activation energy (E_a) of 23.9 kJ mol^{-1} was derived, compared with the turn and strand loss of 37.8 and 42.5 kJ mol^{-1}, respectively. Within the experimental error, these latter two values can be considered as equal.

2.2. β-Hairpin WVYY-^{D}P

Scheme 2 shows the sequence of the β-hairpin WVYY–^{D}P. The sequence is based on the Trpzip2 sequence of Cochran,[1a] with substitution of the Asn–Gly turn by ^{D}Pro–Gly and substitution of the two cross-strand Trp–Trp pairs by Trp–Tyr and Val–Tyr. Thus, the turn rigidity is enhanced and the hydrophobic cross-strand interactions are somewhat weakened, but remain strong enough to assist the folding.[11] The antiparallel β-hairpin structure was confirmed by the FTIR equilibrium data (Figure S1 in the Supporting Information). There is a distinct shoulder in the amide I′ band at 1612 cm^{-1}, which can be assigned to the tertiary Glu–^{D}Pro amide and used as a site-specif-

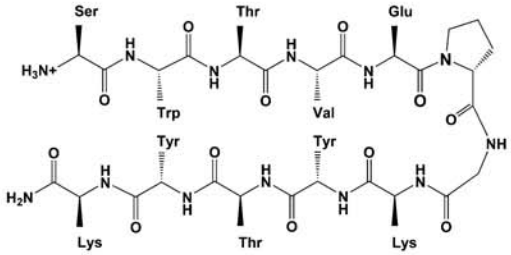

Scheme 2. The sequence of WVYY–^{D}P. The β-hairpin consists of 12 amino acids stabilized by a ^{D}Pro–Gly turn and cross-strand hydrophobic interactions of Trp (W) with Tyr (Y) and Val (V) with Tyr (Y).

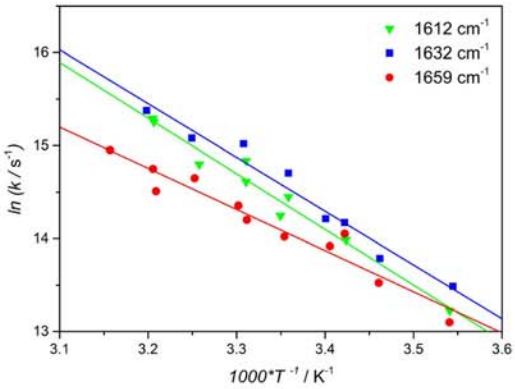

Figure 4. Arrhenius plot for the relaxation kinetics of WVYY–^{D}P. Rates were measured at selected wavenumbers characteristic for strand (1630 cm^{-1}, blue squares), Xxx-^{D}Pro turn region (1612 cm^{-1}, green triangles) and disorder (1663 cm^{-1}, red dots). Lines indicate best fits to the Arrhenius relation as for Figure 3.

ic probe for the turn region. Upon heating, the peptide unfolds reversibly, for which we determined a transition temperature of $T_m \approx 33\,^{\circ}C$ by fitting the temperature-dependent variation of the first component and SVD analysis of the equilibrium FTIR data. The melting temperature (T_m) is much lower than for Trpzip2 ($T_m = 67\,^{\circ}C$ at acidic pH) and also lower than for the previously studied Trpzip2 variants that contained substitutions of just one of the Trp–Trp pairs by either Val or Tyr.[5c,6,11] For the latter variants, two of the four Trp (WWWW) of the Trpzip2 sequence were substituted pairwise (WYWY, WYYW, YWWY, WVVW, VWWV) to modify the hydrophobic cross-strand interactions. All of these formed a β-hairpin structure, but with reduced thermal stability and lower T_m and resembled the substitutions of the peptide studied here in terms of strength of the hydrophobic interactions. The folding of the Trpzip2 variants is driven by cross-strand hydrophobic interactions with minor stabilization by the Asn–Gly turn, which we term "sheet-assisted" folding. In the peptide variant studied here (WVYY–^{D}P) the hairpin folding is additionally enhanced by the ^{D}Pro–Gly turn, which we term as "sheet-assisted and turn-enhanced folding".

The *T*-jump relaxation dynamics were probed at selected wavenumbers derived from the maximum absorbance changes in the FTIR data (Figure S1 in the Supporting Information), namely at 1632 (β-sheet decay), 1659 (rise of disorder), and 1612 cm^{-1} (turn-sheet link). An example of WVYY–^{D}P relaxation and values of all measured time constants are given in the Supporting Information (Figure S2 and Table S1, respectively). Figure 4 summarizes the rates in an Arrhenius plot. The change in the 1659 cm^{-1} component, corresponding to increasing disorder, is again slower than the changes at 1632 and 1612 cm^{-1} for the loss of sheet and the turn-sheet link, respectively. The latter two, related to the strands, have almost the same rates and similar slopes with temperature variation, whereas the former, that is, the gain in disorder, has less slope, and consequently, a lower apparent activation energy.

3. Discussion

3.1. A Comparison between ^{D}P^{D}P and WVYY–^{D}P

Both peptides have relaxation kinetics in the sub-microsecond time range. Table 1 summarizes the relaxation times determined at 25 °C for the decay of the β-sheet probed at 1630 cm^{-1} for ^{D}P^{D}P and at 1632 cm^{-1} for WVYY–^{D}P (β-band), the Xxx–^{D}Pro band probed at 1612 cm^{-1} for both peptides (^{D}P-band) and the rise of the disordered structure probed at 1663 cm^{-1} for ^{D}P^{D}P and at 1659 cm^{-1} for WVYY–^{D}P (disordered). The complete set of our measured relaxation times can be found in the Supporting Information (Tables S1 and S2). As noted in Section 2, for both peptides, the relaxation dynamics of the disordered structure are slower in comparison to those for the strand and turn decay, and overall, the relaxation dynamics of the three-stranded sheet ^{D}P^{D}P are faster than for the hairpin WVYY–^{D}P.

Comparing the relaxation times of WVYY–^{D}P (hundreds of nanoseconds) with those of the Trpzip2 variants WYWY, WYYW, and YWWY (microseconds),[6] the turn influence on the dynamics is clearly observed. For example, at 25 °C, WYWY has a relaxation time of approximately 3.5 μs for the β-sheet component and that of WVYY–^{D}P is approximately 400 ns (Table 1). The strength of hydrophobic interactions for these two hairpins is similar, but the more constrained turn geometry in the ^{D}Pro–Gly turn enhances the relaxation rate for the WVYY–^{D}P hairpin.

From the Arrhenius plots for both peptides (Figures 3 and 4), the rates show no significant difference for the strand (blue) and turn region (green), but slower rates are seen for the disordered state (red). However, there are some noticeable differences: the loss of sheet is systematically faster than the turn-associated change for WVYY–^{D}P, which is not the case for ^{D}P^{D}P, where the fit lines and data points are more overlapped. This suggests that in the case of the WVYY–^{D}P hairpin, the β-sheet change has a faster component than that of the turn (Glu–^{D}Pro turn-to-strand link), whereas in ^{D}P^{D}P, sheet and turn dynamics cannot be differentiated. This difference doesn't have a substantial impact on the apparent activation energies (Table 1), and for both peptides no significant difference can be observed for the fits to the strand (blue) and turn region (green) dynamics within the experimental error. The apparent activation energies that were determined for the rise of disordered

state are smaller than for the loss of strand and change of turn regions, as evidenced by less slope in the Arrhenius plots. Comparing the two peptides, the gain in disorder for the three-stranded β-sheet ^{D}P^{D}P has a lower apparent activation energy (23.8 kJ mol^{-1}) than for the hairpin WVYY–^{D}P (36.8 kJ mol^{-1}). The apparent activation energies were determined from the temperature dependencies of the observed relaxation rates, which must include contributions from both folding and unfolding changes. In a two-state model the rate constants for folding and unfolding can be extracted by using the equilibrium constant (K_{eq}). The folding and unfolding processes can then be described by evaluating their associated activation energies. However, the folding/unfolding mechanism of the peptides studied here is more complex, the transition curves are nonsigmoidal and broad, and separate probes indicate different relaxation processes, thus a multistate mechanism. Nevertheless, we can use the observed rates measured at characteristic wavenumbers and compare their temperature dependence, and apparent activation energies, relative to each other to gain insights into differences in the energy barriers on the energy landscape for different structural components.

3.2. Turn-Initiated and/or Strand-Assisted Folding

The ^{D}Pro–Gly segment is known to facilitate the formation of a stable type II′ β-turn.[12] The ^{D}P^{D}P sequence forms an antiparallel three-stranded β-sheet in aqueous solution without stabilization of the structure by strong cross-strand interactions. The cross-strand residues, Phe–Thr, Thr–Thr, Glu–Lys and Tyr–Leu do not form hydrophobic interactions or a salt bridge at acidic pH. The observed relaxation kinetics are extremely fast (on the sub-microsecond time scale) and agree well with other studies of similar three-stranded peptide sequences.[4] The fast kinetics suggest that ^{D}P^{D}P folding encounters either a relatively small free energy barrier between two distinguishable conformational states or downhill folding without well-defined minima for folded and unfolded states. A previous study of a β-hairpin stabilized by a ^{D}Pro–Gly turn that involved 2D-IR and dispersed vibrational echo (DVE) *T*-jump spectroscopy showed it to also have fast dynamics, again on the sub-microsecond time scale.[13] They proposed a multistep mechanism with the initial steps attributed to the disordering of the cross-strand hydrogen bond contacts of the midstrand region followed by unfolding of the rest of the peptide strand structure, except for the turn region, which does not undergo significant structural variations.

If the folding initiated by the ^{D}Pro–Gly turn is assisted by hydrophobic cross-strand interactions of the strands, the kinetics are still in the sub-microsecond time scale, but are slower, as we have measured for WVYY–^{D}P (Table 1 and the Supporting Information). Studies of the dynamics associated to the collapse of the hydrophobic side chains have been reported previously for other β-sheet peptides with ^{D}Pro–Gly turns[4a,b] or cross-linking modifications near the turn region.[14] The nucleation of the hairpin should be slower as the solvent molecules must be displaced to facilitate the formation of cross-strand hydrophobic interactions and hydrogen bonds in the folding mechanisms. The apparent activation energies measured for WVYY–^{D}P are higher than for ^{D}P^{D}P (Table 1), which is consistent with the reduced rates for WVYY–^{D}P. The folding of the WVYY–^{D}P β-hairpin is turn-enhanced and strand-assisted and its kinetics reflect the contribution of different forces from the turn and the hydrophobic residues.

The turn has a strong influence on β-sheet folding, as many studies have shown.[5,7] However, a hairpin can be stabilized, mainly by the hydrophobic interactions of the strands, and have a weak turn-promoting sequence, as is the case for Trpzip2 and its variants. The hydrophobic interactions in Trpzip2 are significantly stronger than those in WVYY–^{D}P, but the Asn–Gly turn is a much weaker turn promoter than ^{D}Pro–Gly. The kinetics for solely strand-assisted hairpin folding are significantly slower (microseconds), again reflecting the effects of turn and strand stabilization.

3.3. ^{D}Pro as Site-Specific IR Probe

The distinct amide I′ component of the Xxx–^{D}Pro amide group provides the possibility of studying site-specific dynamics of the turn region with residue-specific resolution. For both peptides, ^{D}P^{D}P and WVYY–^{D}P, we measured the same dynamics for the Xxx–^{D}Pro amide as for the overall β-strand components (Table 1). One reason might be that the central part of the turn is not probed directly, rather the turn-to-strand link is sensed and that matches the β-strand dynamics. It would be interesting to determine if Gly–^{D}Pro turns might provide a suitable probe for turn dynamics in the center of the turn, while still contributing to the stability of the turn.

4. Conclusions

Our studies illustrated the interplay between turn stability and cross-strand hydrophobic interactions in influencing the kinetics of β-sheet folding. The contribution of different forces to the nucleation of a hairpin in the β-sheet folding process was reflected by differences in the *T*-jump relaxation kinetics. Hairpin formation that is nucleated by a turn is expected to be intrinsically rapid for a strong turn, as the folding process is driven by local forces at the turn. This was confirmed by the fast dynamics of the three-stranded β-sheet ^{D}P^{D}P, which is stabilized by two rigid ^{D}Pro–Gly turns. For a hairpin with additional hydrophobic cross-strand interactions, the folding process must involve hydrophobic collapse, resulting in slower nucleation, as solvent molecules must be displaced, structural rearrangements occur, and interactions of the hydrophobic residues must be formed. The β-hairpin WVYY–^{D}P, which is stabilized by one constrained ^{D}Pro–Gly turn plus modest hydrophobic cross-strand interactions (Trp–Tyr, Val–Tyr), revealed dynamics that were still on the sub-microsecond time scale, but slower than those of ^{D}P^{D}P. If the hydrophobic interactions of the sheets are the main contributors to stabilizing a hairpin and the turn is weakly promoted, the hydrophobic collapse mediated dynamics lead to significantly slower folding, on the microsecond time scale, which has been observed by many groups for Trpzip2 variants, β-hairpins that are stabilized by

hydrophobic residues, and the less rigid Asn-Gly turn. The weaker turn-promoting sequence does not enhance the strand-assisted folding.

Experimental Section

Peptide Synthesis and Sample Preparation

The WVYY—^{D}P peptide sample was synthesized at the University of Illinois at Chicago (UIC) using standard Fluorenylmethoxycarbonyl (Fmoc)-based solid-state methods.[15] Crude peptides were purified by HPLC. The ^{D}P^{D}P peptide was obtained from SciLight Biotechnology LLC, Beijing, China. To eliminate spectral interference from trifluoroacetate counterions remaining from the peptide synthesis, peptides were dissolved in 0.1 M DCl and lyophilized three times. After lyophilization, the peptide ^{D}P^{D}P was redissolved in a 20 mM deuterated phosphate buffer at a concentration of 20 mg mL^{-1} and adjusted to pD ≈ 5 by the addition of DCl. The β-hairpin WVYY–^{D}P was dissolved at 20 mg mL^{-1} in D_2O (pD ≈ 1.5).

FTIR Spectra at Thermal Equilibrium

The FTIR spectra were acquired with a Bruker Equinox 55 FTIR spectrometer (Bruker, Germany) equipped with a mercury cadmium telluride (MCT) detector. At each temperature, 128 scans with a spectral resolution of 4 cm^{-1} were averaged for one FTIR spectrum. The acquisition of each set of spectra was carried out in the temperature range of 7–85 °C in steps of $\Delta T \approx 5$ °C. The temperature of the sample holder was controlled by a water bath (Lauda Ecoline E300, Germany) and the exact temperature of the sample cell was recorded by a Pt100 sensor. A home-built software-controlled shuttle device was used to measure the sample and reference signal successively for each temperature.

Temperature-Jump Experiments and Spectrometer Setup

Relaxation methods allow the fast relaxation of a system into a new equilibrium state after a previous disturbance to be monitored. This can be initiated by a rapid change in pressure, temperature, or another physical quantity related to the equilibrium constant. We use the laser-excited, direct solvent absorbance initiated temperature-jump technique for time-resolved studies of peptide folding. One of the main advantages of this method is the absence of any additives in the sample, which are used in other studies,[16] to initiate the rapid increase of the sample temperature. In this way any disturbing chemical or spectral interactions between the additive and sample are avoided. Moreover, a distinct vibrational band of the solvent can be excited in a spectral region where the peptide has no absorbance. The choice of the band is dependent on the solvent used (e.g. H_2O, D_2O, and MeOH), the peptide sample (solubility) and the available excitation wavelengths (of the pump laser). Frequency and intensity variations in the amide I region reflect changes in the secondary structure of polypeptides. By monitoring the spectral changes at single wavelengths, it is possible to differentiate the dynamics for different secondary-structure components, for example, β-sheets or α-helices.

Figure 5 shows a schematic drawing of our laser spectrometer. To generate a rapid increase of temperature in the D_2O-based sample, the fundamental (1064 nm) of a Q-switched Nd:YAG laser (5 ns full width at half maximum, 700 mJ, Continuum, Excel Technology, Europe) was Raman shifted to 1.9 μm. The 1.06 μm laser pulse was focused into the Raman shifter, a gas cell (Radiant Dyes, Cologne, Germany) filled with H_2 gas at 30 bar as the active medium. Raman shifting produced several (Stokes and Anti-Stokes) lines simultaneously, which were then separated by a Pellin-Broca prism. The Stokes line at 1909 nm (5238 cm^{-1}) was used to excite an overtone of the stretching vibration of the D_2O solvent and to heat the illuminated sample volume rapidly. Filters and apertures prevented the other Raman-shifted lines and scattered light from reaching the sample chamber and interfering with the probe beam, as well as from hitting the detector element and risking damage.

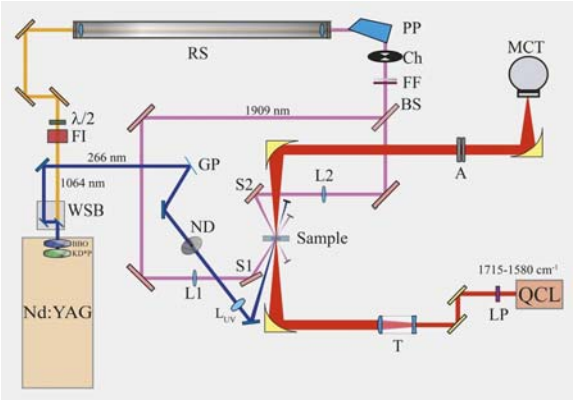

Figure 5. IR spectrometer setup. The home-built spectrometer was used to monitor the relaxation kinetics that were either triggered by a *T*-jump (excitation at 1909 nm) or by a photochemically induced pH-jump (excitation at 266 nm). QCL: quantum cascade laser tunable between 1715–1580 cm^{-1}, probe laser; LP: long pass filter; T: telescope; A: attenuator; MCT: photovoltaic HgCdTe detector; Nd:YAG: Q-switched Nd:YAG laser, pump laser; WSB: wavelength separation box; FI: Faraday isolator; $\lambda/2$: $\lambda/2$ plate; RS: Raman shifter; PP: Pellin–Broca prism; Ch: chopper; FF: color filters; BS: beam splitter; L1, L2: focusing lenses for the pump pulse at 1909 nm; BBO, KD*P: nonlinear crystals for fourth harmonic (266 nm) generation; GP: glass plate; ND: neutral density attenuator; L_{UV}: focusing lens for 266 nm pump pulse.

The NIR pump pulse was split by a 50:50 beam splitter into two counter-propagating beams, leading to homogeneous sample heating at the sample to minimize cavitation, with one delayed by 5 ns, the pulse length of the Nd:YAG laser. The small absorbance coefficient of D_2O at 5238 cm^{-1} in combination with counter-propagation by two subsequently arriving pump pulses prevented unwanted temperature gradients in the excited sample volume. The pump beams were focused behind the sample cell, to avoid burning the sample–cell interface, by use of two CaF_2 lenses and were adjusted by dichroic mirrors to overlap spatially, thus forming a heated area (Ø ~2 mm) in the center of the sample. The pump energy excites the solvent on the time scale of ps[9] and the final temperature is reached within the 10 ns pumping length of the two consecutive 5 ns heating pulses.

An additional excitation branch (Figure 5; dark-blue beam line) was added to enable measurement of photochemically-induced pH-jump relaxation kinetics.[17] This technique allowed the study of pH-sensitive conformational changes of the proteins.[18] Dissolved *o*-nitrobenzaldehyde, a photoreactive compound, can for example be used as caged proton source that releases protons rapidly after irradiation by a UV light pulse.[19] The excitation pulse was provided by generation of the fourth harmonic at 266 nm of a Q-switched Nd:YAG laser. The intensity of the 266 nm pump pulse and illuminated area controlled the amount of free protons produced in the sample per pulse and in this manner adjusted the size of the pH-jump in the excited volume.

To probe the relaxation kinetics in the amide I region, a quantum cascade laser (QCL, Daylight Solutions Inc., USA) was used as a tunable cw IR source. The mid infrared emission could be tuned between 1715 and 1580 cm^{-1} to obtain a single wavelength output with a narrow line width (< 100 MHz). The QCL was built with an external cavity in a Littrow configuration, allowing the suppression of all laser modes except for the particular mode needed for the measurement. The probe laser provides energies up to about 100 mW, depending on wavenumber and the applied current. The high power output of the QCL, as the IR probe source, has a dramatically improved signal-to-noise ratio, as compared with that of the formerly used lead salt diodes.[20] The laser beam was focused on a probe spot (Ø ~ 300–400 μm) that was significantly smaller than the excitation spot used for the *T*-jump or pH-jump.

There are different approaches to separate solvent from peptide dynamics,[16,21] one of which is to measure the solvent separately and to subtract it, which is the approach that we used in this study. The absorbance change of the solvent after the *T*-jump is much higher than that of the peptide of our samples, thus tracking relatively small peptide absorbance changes upon unfolding requires that the subtraction of the solvent contribution is done as precisely as possible. Due to the small probe volume we used, the absolute absorbance value was sensitive to the sample position and slight differences in sample positioning could cause big errors when measuring the solvent reference. Thus, we used a refillable cell composed of two CaF_2 windows separated by a Teflon spacer with a path length of 100 μm (Figure 6). To allow simple exchange of the solvent by the peptide sample, the top window was equipped with two holes, one of them connected by a tube for pipetting. To minimize the peptide sample required, the volume of the cell was adjusted to ≈10 μL, by limiting the aperture. The cell openings were sealed for the measurements to prevent evaporation and loss of the sample in the cell. Firstly, the entire series of *T*-jump experiments with different starting temperatures was measured for only the solvent. Next, the cell was refilled with the peptide sample and the same series of *T*-jump experiments was performed. The averaged solvent transients were subtracted from the averaged peptide (plus solvent) transients resulting in the pure peptide kinetics without the solvent contributions and/or the convoluted instrument response.

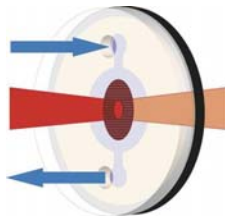

Figure 6. Refillable cell for *T*-jump experiments. The cell consists of two CaF_2 windows separated by a Teflon spacer. Two holes were drilled in one window allowing the exchange of the reference and sample solutions without changing the alignment of the pump and probe beams and their overlap in the cell. Darker area schematically represents the region excited by the pump beam, and red spot in the center that probed by the QCL beam. For FTIR measurements a non-refillable cell consisting of two plane CaF_2 windows (no holes) was used.

The main advantage of the refillable cell is the ability to obtain the exact same configuration and position of the CaF_2 cell with respect to the overlap adjustment of the pump and probe beams in the excited sample volume, as the exact positioning of the beams is crucial for the quality of the *T*-jump experiments.[22] We additionally tested a home-built split cell consisting of two compartments, one for the solvent and the other filled with the peptide sample, modeled on a cell geometry that has been used before.[23] An advantage of a split cell is that both peptide and solvent are thermally equilibrated in one cell, and thus, have the same starting temperature for the *T*-jump experiments. However, we found that the major drawback of the split cell was that lateral translation of the split cell resulted in a different overlap of the beams within the cell in our setup. This effect could be minimized by readjustment of the angle between the cell and the probe beam, but this could not always be achieved perfectly and in addition was time consuming, as it had to be done at each repositioning step. Moreover, the compartments in our design had a slightly different path length, due to uneven window and spacer surfaces. In both cell configurations (refillable and split), the final *T*-jump magnitude and final temperature could be controlled with an overall error of $\Delta T = 1–2\,^{\circ}C$. Better reproducibility of the results was obtained by use of the refillable cell, which was employed in this study.

After passing through the sample, the IR probe beam was redirected and refocused onto a fast, liquid-N_2-cooled photovoltaic HgCdTe detector (18 MHz, KMPV11–1 J2, Kolmar Technologies, USA, 19 ns response time). To operate the QCL in a stable mode, the high energy density of the probe beam had to be attenuated to prevent damage of the detector element. Several apertures and bandpass filters were introduced into the beam path, as scattered light and thermal radiation from the heated sample can perturb the signal. Scattered light may also be back-reflected into the laser optics, thus causing damage to the QCL. The entire spectrometer setup was encased in purpose-built boxes and purged with dried air to minimize the absorbance of water vapor in the MIR. The signal was digitized by a transient recorder board (16 bit, 105 MHz, Spectrum, Germany), triggered by the TTL signals from the Nd:YAG laser. The time interval was evaluated up to 1.2 ms. Usually around 2000 transients were averaged to reduce noise before further evaluating the data.

To account for the background signal, a chopper was synchronized to the pump laser to create different illumination conditions for a series of pulses. Correction for a reference signal S(-/+) (without pump, with probe) was necessary to eliminate any remaining electronic distortion signals, as well as background light contributions at the detector. Additionally, a signal without pump and without probe light [S(-/-)] was recorded. The reference signals [S (-/+), S(-/-)] were used for the proper calculation of the transient absorbance changes (ΔA). To exclude distorted transients caused by cavitation effects, a self-developed software filter (MATLAB2010, The MathWorks, MA, U.S.A.) was applied to sort out the most reliable data after collection. The final solvent-corrected transient traces for each temperature were further subjected to an averaging procedure, so that an equal number of points were distributed in each time decade (20 points per decade). This resulted in a significant reduction of signal distortions, such as detector ringing and thermal lensing effects. Furthermore, the fast time points were then not underrepresented in the fit procedure, as is often the case with linear signal recording. These modifications allowed the fast time range between 100–200 ns to be investigated, which improved the quality of the final transient data. This method ensured a more reliable fitting of transient spectra on a logarithmic time scale.

The magnitude of the instantaneous absorbance change (ΔA) after the laser pulse was used to determine the related *T*-jump. The final temperature of the peptide (after the *T*-jump) was calculated by referencing the temperature change to the temperature dependent FTIR spectra of the solvent at the wavenumber and initial sample temperature used for the measurement. Solvent and peptide sample kinetics were recorded separately as described above. The solvent kinetics were scaled before the subtraction from the peptide signal. Due to the remaining distorted signal in the early phase for the 1663 cm^{-1} measurements, the data for $^{D}P^{D}P$ could only be fitted from 270–500 ns to 1.2 ms, whereas the 1630 and 1612 cm^{-1} measurements were evaluated starting from 160 ns. The

WVYY–^{D}P data for 1612, 1632, and 1659 cm^{-1} were evaluated from 150–300 ns up to 1.2 ms depending on the quality of the transients. A monoexponential decay function $\Delta A = A_0 + A_1 \cdot e^{-t/\tau}$ was sufficient to fit both the three-stranded β-sheet ^{D}P^{D}P and the β-hairpin WVYY-^{D}P data for all probed wavenumbers.

Acknowledgements

We gratefully acknowledge financial support by the Deutsche Forschungsgemeinschaft (SFB 969 to K.H.), the Center of Applied Photonics Konstanz (to K.H.), the Alexander von Humboldt Foundation (Humboldt Research Award to T.A.K.), and the National Science Foundation of China (NSFJ BK20140449 to H.C.).

Keywords: conformational dynamics · IR spectroscopy · peptides · protein folding · temperature jump

[1] a) A. G. Cochran, N. J. Skelton, M. A. Starovasnik, *Proc. Natl. Acad. Sci. USA* **2001**, *98*, 5578–5583; b) S. H. Gellman, *Curr. Opin. Chem. Biol.* **1998**, *2*, 717–725; c) R. M. Hughes, M. L. Waters, *Curr. Opin. Struct. Biol.* **2006**, *16*, 514–524.

[2] H. L. Schenck, S. H. Gellman, *J. Am. Chem. Soc.* **1998**, *120*, 4869–4870.

[3] S. V. Kuznetsov, J. Hilario, T. A. Keiderling, A. Ansari, *Biochemistry* **2003**, *42*, 4321–4332.

[4] a) R. P. Y. Chen, J. J. T. Huang, H. L. Chen, H. Jan, M. Velusamy, C. T. Lee, W. S. Fann, R. W. Larsen, S. I. Chan, *Proc. Natl. Acad. Sci. USA* **2004**, *101*, 7305–7310; b) N. N. W. Kuo, J. J. T. Huang, J. Miksovska, R. P. Y. Chen, R. W. Larsen, S. I. Chan, *J. Am. Chem. Soc.* **2005**, *127*, 16945–16954; c) Y. Xu, P. Purkayastha, F. Gai, *J. Am. Chem. Soc.* **2006**, *128*, 15836–15842.

[5] a) T. Takekiyo, L. Wu, Y. Yoshimura, A. Shimizu, T. A. Keiderling, *Biochemistry* **2009**, *48*, 1543–1552; b) C. D. Tatko, M. L. Waters, *J. Am. Chem. Soc.* **2002**, *124*, 9372–9373; c) L. Wu, D. McElheny, R. Huang, T. A. Keiderling, *Biochemistry* **2009**, *48*, 10362–10371.

[6] A. Popp, L. Wu, T. A. Keiderling, K. Hauser, *J. Phys. Chem. B* **2014**, *118*, 14234–14242.

[7] L. Wu, D. McElheny, V. Setnicka, J. Hilario, T. A. Keiderling, *Proteins Struct. Funct. Bioinf.* **2012**, *80*, 44–60.

[8] a) R. B. Dyer, O. Einarsdottir, P. M. Killough, J. J. Lopezgarriga, W. H. Woodruff, *J. Am. Chem. Soc.* **1989**, *111*, 7657–7659; b) R. B. Dyer, F. Gai, W. H. Woodruff, *Acc. Chem. Res.* **1998**, *31*, 709–716.

[9] a) P. A. Anfinrud, C. Han, R. M. Hochstrasser, *Proc. Natl. Acad. Sci. USA* **1989**, *86*, 8387–8391; b) T. Elsaesser, W. Kaiser, *Annu. Rev. Phys. Chem.* **1991**, *42*, 83–107; c) L. Genberg, F. Heisel, G. McLendon, R. J. D. Miller, *J. Phys. Chem.* **1987**, *91*, 5521–5524.

[10] a) J. Hilario, J. Kubelka, T. A. Keiderling, *J. Am. Chem. Soc.* **2003**, *125*, 7562–7574; b) P. Xie, M. Diem, *J. Am. Chem. Soc.* **1995**, *117*, 429–437.

[11] L. Wu, D. McElheny, T. Takekiyo, T. A. Keiderling, *Biochemistry* **2010**, *49*, 4705–4714.

[12] a) F. A. Syud, J. F. Espinosa, S. H. Gellman, *J. Am. Chem. Soc.* **1999**, *121*, 11577–11578; b) T. S. Haque, S. H. Gellman, *J. Am. Chem. Soc.* **1997**, *119*, 2303–2304; c) H. E. Stanger, S. H. Gellman, *J. Am. Chem. Soc.* **1998**, *120*, 4236–4237; d) H. E. Stanger, F. A. Syud, J. F. Espinosa, I. Giriatt, T. Muir, S. H. Gellman, *Proc. Natl. Acad. Sci. USA* **2001**, *98*, 12015–12020; e) S. R. Raghothama, S. K. Awasthi, P. Balaram, *J. Chem. Soc. Perkin Trans. 2* **1998**, 137–143.

[13] A. W. Smith, A. Tokmakoff, *Angew. Chem. Int. Ed.* **2007**, *46*, 7984–7987; *Angew. Chem.* **2007**, *119*, 8130–8133.

[14] B. N. Markiewicz, L. Yang, R. M. Culik, Y. Q. Gao, F. Gai, *J. Phys. Chem. B* **2014**, *118*, 3317–3325.

[15] H. Chi, PhD thesis, University of Illinois at Chicago, Chicago, IL **2013**.

[16] A. P. Ramajo, S. A. Petty, M. Volk, *Chem. Phys.* **2006**, *323*, 11–20.

[17] D. T. Clarke, A. J. Doig, B. J. Stapley, G. R. Jones, *Proc. Natl. Acad. Sci. USA* **1999**, *96*, 7232–7237.

[18] a) T. P. Causgrove, R. B. Dyer, *Chem. Phys.* **2006**, *323*, 2–10; b) M. L. Donten, P. Hamm, *Chem. Phys.* **2013**, *422*, 124–130; c) S. Abbruzzetti, E. Crema, L. Masino, A. Vecli, C. Viappiani, J. R. Small, L. J. Libertini, E. W. Small, *Biophys. J.* **2000**, *78*, 405–415; d) S. Abbruzzetti, S. Sottini, C. Viappiani, J. E. T. Corrie, *Photochem. Photobiol. Sci.* **2006**, *5*, 621–628; e) M. L. Donten, S. Hassan, A. Popp, J. Halter, K. Hauser, P. Hamm, *J. Phys. Chem. B* **2015**, *119*, 1425–1432.

[19] M. L. Donten, P. Hamm, J. VandeVondele, *J. Phys. Chem. B* **2011**, *115*, 1075–1083.

[20] C. Krejtschi, R. Huang, T. A. Keiderling, K. Hauser, *Vib. Spectrosc.* **2008**, *48*, 1–7.

[21] a) S. Nagarajan, H. Taskent-Sezgin, D. Parul, I. Carrico, D. P. Raleigh, R. B. Dyer, *J. Am. Chem. Soc.* **2011**, *133*, 20335–20340; b) C. Y. Huang, J. W. Klemke, Z. Getahun, W. F. DeGrado, F. Gai, *J. Am. Chem. Soc.* **2001**, *123*, 9235–9238.

[22] W. O. Wray, T. Aida, R. B. Dyer, *Appl. Phys. B* **2002**, *74*, 57–66.

[23] S. Williams, T. P. Causgrove, R. Gilmanshin, K. S. Fang, R. H. Callender, W. H. Woodruff, R. B. Dyer, *Biochemistry* **1996**, *35*, 691–697.

Manuscript received: November 30, 2015
Accepted Article published: January 20, 2016
Final Article published: February 5, 2016